Journal of Biomolecular NMR, **13:** 275–288, 1999.
KLUWER/ESCOM

Microsecond time scale dynamics in the RXR DNA-binding domain from a combination of spin-echo and off-resonance rotating frame relaxation measurements

Frans A.A. Mulder, Paul J.A. van Tilborg, Robert Kaptein & Rolf Boelens*
Bijvoet Center for Biomolecular Research, Utrecht University, Padualaan 8, 3584 CH Utrecht, The Netherlands

Received 19 August 1998; Accepted 4 December 1998

Key words: adiabatic pulses, chemical exchange, CPMG, DNA-binding protein, off-resonance relaxation, protein dynamics, retinoid X receptor, zinc finger

Abstract

Slow protein dynamics can be studied by ^{15}N spin-echo (CPMG) and off-resonance rotating frame relaxation through the effective field dependence of the exchange-mediated relaxation contribution. It is shown that, by a combination of these complementary techniques, a more extended sampling of the microsecond time scale processes is achieved than by either method alone. ^{15}N R_2 and improved off-resonance $R_{1\rho}$ experiments [Mulder et al. (1998) *J. Magn. Reson.*, **131**, 351–357] were applied to the 9-*cis*-retinoic acid receptor DNA-binding domain and allowed the identification of 14 residues exhibiting microsecond time scale dynamics. Assuming exchange between two conformational substates, average lifetimes ranging from 37 to 416 μs, and chemical shift differences of up to 3 ppm were obtained. The largest perturbation of tertiary structure was observed for the second zinc finger region, which was found to be disordered in the solution structure [Holmbeck et al. (1998) *J. Mol. Biol.*, **281**, 271–284]. Since this zinc-coordinating domain comprises the principal dimerization interface for RXR in a wide repertoire of complexes with different hormone receptors to their cognate response elements, this finding has important implications for our understanding of nuclear receptor assembly on DNA direct repeats. The flexibility observed for the dimerization domain may explain how RXR, through the ability to adaptively interact with a wide variety of highly homologous partner molecules, demonstrates such a versatile DNA-binding repertoire.

Abbreviations: RXR, retinoid X receptor; CPMG, Carr–Purcell–Meiboom–Gill; DD, dipole-dipole; CSA, chemical shift anisotropy; HRE, hormone response element; R_2, transverse relaxation rate; $R_{1\rho}$, rotating frame relaxation rate; R_1, longitudinal relaxation rate; $R_{2,ex}$, exchange-mediated transverse relaxation rate; DR, direct repeat; BPTI, bovine pancreatic trypsin inhibitor.

Introduction

It is widely recognized that proteins undergo significant internal motions on a broad range of time scales. This dynamical behavior can play an important role in biological processes, such as protein folding, enzyme action and molecular recognition (see, for example, Hirs and Timasheff, 1986; Karplus and McCammon, 1986). Therefore, considerable effort has been devoted to the study of biomolecular mobility from the analysis of backbone ^{15}N relaxation due to dipolar and CSA interactions (reviewed, for example, by Torchia et al., 1993; Wagner et al., 1993; Peng and Wagner, 1994a,b). As the ^{15}N relaxation rates depend on the random reorientational behavior of the ^{15}N-^{1}H bond vector they serve as probes of internal motions that are faster than the overall tumbling time of the molecule; for proteins studied by NMR this typically refers to the picosecond to nanosecond regime. In contrast, relatively few experiments for measuring motions on intermediate time scales (millisecond to microsecond)

*To whom correspondence should be addressed. E-mail: boelens@nmr.chem.uu.nl

have been designed or applied to proteins. Movements on these time scales may contribute to transverse relaxation through the fluctuation of the chemical environment of a nucleus, a phenomenon generally referred to as 'chemical exchange'. This relaxation mechanism is effective when the motion causing the chemical shift perturbation has a frequency that is on the order of the difference in the resonance frequencies corresponding to the different sampled chemical surroundings. Consequently, slow motions in proteins are often signalled from (i) an anomalous increase in R_2 for a particular residue, or set of residues, with respect to the body of the molecule; (ii) the requirement of $R_{2,ex}$ terms in model-free fitting due to inconsistencies with other relaxation parameters (Palmer et al., 1991); or (iii) the dependence of $R_{2,ex}$ on the square of the static magnetic field strength (Phan et al., 1996; Vis et al., 1998). Although useful indicators of slow motions, these methods cannot delineate the dynamics in terms of time constants and chemical shift differences. A detailed description of these parameters can, however, be obtained from the analysis of exchange-mediated relaxation in the presence of additional rf fields. This information is of profound interest, first, because the chemical shift provides a valuable probe of macromolecular structure (Wishart et al., 1991), and second, because kinetic rate constants can be used to obtain activation enthalpies (Mandel et al., 1996).

Two related methods have recently been applied to the detailed analysis of intermediate time scale dynamics from ^{15}N relaxation in proteins: (a) measurement of decay rates in the presence of spin-echo pulse trains of variable spacing, such as CPMG experiments (Orekhov et al., 1994; Meekhof et al., 1998), and (b) measurements of spin-lattice relaxation in the rotating frame as a function of the effective field strength (Szyperski et al., 1993; Akke and Palmer, 1996; Zinn-Justin et al., 1997; Akke et al., 1998). Several analytical expressions have been derived to relate the spin-echo decay rate to the refocusing pulse repetition rate (Luz and Meiboom, 1963; Bloom et al., 1965), which allows quantification of rate processes that are on the order of the pulse repetition rate, typically 10^2 to 10^4 s^{-1}. The dependence of the rotating frame relaxation rate on the exchange kinetics has been derived for cases where the rf field is applied (a) on-resonance (Meiboom, 1961; Deverell et al., 1970), and (b) off-resonance (Strange and Morgan, 1970; Davis et al., 1994) with the spins. Whereas the on-resonance variant is suitable for the study of rate constants on the order of 10^2 to 10^4 s^{-1}, application of the rf field off-resonance has extended this range up to approximately 10^5 s^{-1}. A hybrid approach, extracting the motional parameters of the exchange process from the simultaneous analysis of CPMG R_2 and (off-resonance) $R_{1\rho}$ data, has not yet been reported. It was deemed useful to assess how a combination of these approaches can be used to allow for a better description of the intermediate time scale motions.

As part of an ongoing study of the dynamical behavior of nuclear receptor proteins, ^{15}N CPMG R_2 and off-resonance $R_{1\rho}$ relaxation experiments were applied to the DNA-binding domain of the nuclear hormone receptor RXR, for which intermediate time scale dynamics were inferred from ^{1}H and ^{15}N transverse relaxation data (van Tilborg et al., 1998). The goal of the research was to investigate whether flexibility could account for regions of the protein that were found to be disordered in solution (Lee et al., 1993; Holmbeck et al., 1998), but well defined in the crystal structure of a complex with TR on a DR4 response element (Rastinejad et al., 1995). It was hoped that this would provide additional insight into the ability of RXR to interact with a variety of homologous nuclear receptors, and with a wide repertoire of DNA-binding motifs.

Theory

Intramolecular (conformational) exchange refers to a process in which a nucleus interchanges between different chemical environments. In the following, a two-state process is assumed between sites A and B, separated in chemical shift by $\delta\omega = 2\pi\delta\nu$, and having populations p_A and p_B and forward and backward rate constants k_1 and k_{-1}, respectively. The exchange rate is expressed as $k_{ex} = k_{-1}/p_A = k_1/p_B$, and the exchange correlation time is defined as $\tau_{ex} = 1/k_{ex}$, representing the mean lifetime of the two states. Random jumps between the magnetically different sites will lead to dephasing of the spin coherences. Since the time-dependent perturbation relaxes the system only insofar as it does not commute with the Zeeman Hamiltonian, chemical exchange only contributes to transverse relaxation (Jacquinot and Goldman, 1973).

Several theories have been put forward to describe the evolution of the density matrix in the presence of spin-echo (CPMG) pulse trains, or in the presence of rf fields. The two principal techniques will be discussed below.

The determination of chemical-exchange rates from spin-echo measurements

Various approaches have been followed to describe the effect of spin-echo pulses on exchange-mediated relaxation (Luz and Meiboom, 1963; Bloom et al., 1965). We reproduce here the equations put forward by Bloom et al. (1965), following conventions of notation used by Palmer et al. (1996). However, we express the relaxation equation in terms of the average field strength of the CPMG train, ν_{CPMG}, defined by the rate at which we apply 360° rotations to the magnetization. This definition is used to stress the similarities, and to compare, in an easy way, the sampling provided by spin-echo and spin-lock methods, as will become apparent. The relaxation contribution $R_{2,ex}$ brought about by the exchange process can be expressed in terms of the CPMG frequency, under experimental control, and the desired parameters of the exchange process:

$$R_{2,ex} = \frac{k_{ex}}{2} - 2\nu_{CPMG}\sinh^{-1}\left(\frac{k_{ex}}{\xi}\sinh\frac{\xi}{4\nu_{CPMG}}\right) \quad (1)$$

where $\xi = (k_{ex}^{-2} - 4p_A p_B \delta\omega^2)^{1/2}$. Numerical simulations indicate that this equation is accurate provided $(p_A p_B)^{1/2}\delta\omega/k_{ex} < 0.2$, i.e. in the fast exchange limit, which is well satisfied in the simulations and experimental data presented. The dependence of $R_{2,ex}$ on ν_{CPMG} and k_{ex} is illustrated in Figure 1. Panel a shows a contour plot of Equation 1 as a function of the effective field and exchange rate. The main characteristics are illustrated by the cross sections depicted as solid lines in panels c and d, respectively. First, panel c exemplifies how the CPMG relaxation rate is a very sensitive probe to fast processes, even at moderate pulse repetition rates. Furthermore, the exchange contribution is minimized when the phases of the spins are inverted increasingly rapidly. This phenomenon has recently stimulated the development of improved heteronuclear magnetization transfer steps in multidimensional NMR (Mueller et al., 1995; Mulder et al., 1996). Second, $R_{2,ex}$ is a decreasing function of k_{ex} for large values of k_{ex}/ν_{CPMG}, but an increasing function of k_{ex} for small values of k_{ex}/ν_{CPMG}. This behavior, illustrated in panel d, is due to two opposing effects. For free precession in the fast exchange limit the relaxation rate is always a decreasing function of k_{ex}, reflecting the well-known fact that line-broadening is reduced as we move away from coalescence. Conversely, the rf field reduces most strongly the exchange-mediated relaxation of slowly interconverting spins.

Equation 1 can be greatly simplified in the slow pulsing limit. First, for values of $\nu_{CPMG} < 0.1k_{ex}$, the exchange-mediated relaxation becomes linearly dependent on the pulse rate (Luz and Meiboom, 1963):

$$R_{2,ex} = (1 - 4\nu_{CPMG}/k_{ex})p_A p_B \delta\omega^2/k_{ex} \quad (2)$$

Second, under the condition $\nu_{CPMG} \ll 0.1k_{ex}$ this result reduces further to the familiar expression for the free precession limit:

$$R_{2,ex} = p_A p_B \delta\omega^2/k_{ex} \quad (3)$$

Scalar coupling has not been taken into account in the above derivations. In the case of homonuclear spins the creation of anti-phase magnetization leads to a modulation of the echo intensity by an effective, ν_{CPMG}-dependent J-coupling (Allerhand, 1966). For a heteronuclear spin system, coupling of the heteronucleus with the proton spin may still produce anti-phase coherence, which has different relaxation properties. This coupling is effectively suppressed if CPMG experiments are performed with rapid spin-echo pulsing, keeping to the condition $\nu_{CPMG} \geq 5J$, and the relaxation can be considered exclusively due to the in-phase component (Peng et al., 1991b; Kay et al., 1992; Palmer et al., 1992). On the other hand, the pulse rate should be limited: first, as long as the echo pulses are short with respect to the periods of free precession, relaxation during the pulses can be neglected. Second, high pulse repetition rates are usually avoided because of limited amplifier duty cycle or to prevent heating. In practice, experiments are performed in a working range of $450 \leq \nu_{CPMG} \leq 1250$ Hz.

The determination of chemical-exchange rates from spin-lock measurements

Most examples in the literature dealing with the determination of exchange kinetics via $R_{1\rho}$ measurements use the equations derived by Deverell et al. (1970). In the presence of an rf field of magnitude $\omega_1 = \gamma B_1 = 2\pi\nu_1$, applied on-resonance with the spins, the relaxation rate is given by:

$$R_{2,ex} = p_A p_B \delta\omega^2 \frac{k_{ex}}{k_{ex}^2 + \omega_1^2} \quad (4)$$

where the angular velocity of the rf field, ω, is chosen to coincide with the center of gravity of the exchange-averaged resonance lines. A lower limit, $\omega_1 \gg \delta\omega$, is imposed on the strength of the rf field, in order for the spin magnetizations, corresponding to the different resonance frequencies of the interconverting species,

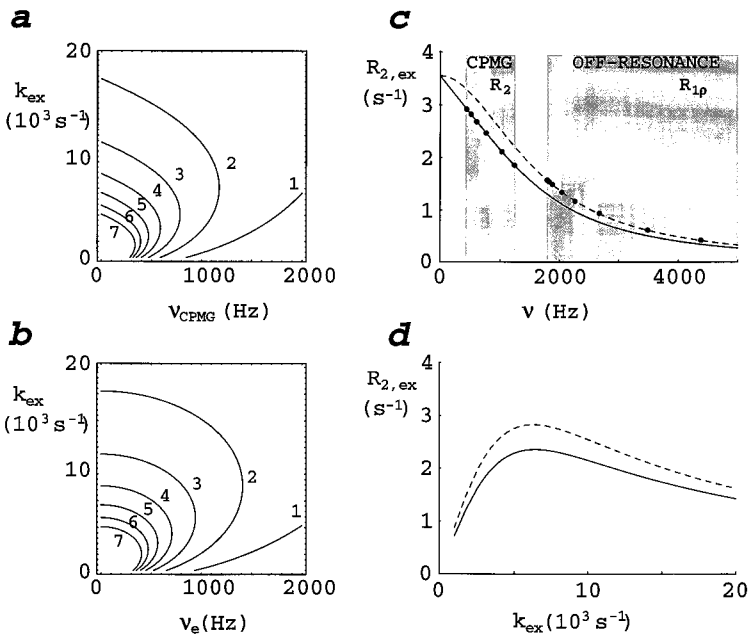

Figure 1. Representations of the chemical exchange-mediated transverse relaxation rate $R_{2,ex}$ in the presence of spin-echo pulses or a continuous rf spin-lock field. Contour plots (a,b) represent $R_{2,ex}$ as a function of the exchange rate k_{ex} and the effective field ν (in frequency units), in the presence of pulsed (a) or continuous (b) rf irradiation. Contour levels have been drawn for values of $R_{2,ex}$ ranging from 1 to 7 s^{-1}. Panels c and d show cross-sections of the 3D surfaces at $k_{ex} = 10^4$ s^{-1} and $\nu = 10^3$ Hz, respectively. Curves represent CPMG (full) and off-resonance rotating frame (dashed) relaxation rates. Closed circles illustrate the sampling employed in experiment. In (a,c) ν is given by $\nu_{CPMG} = (2\tau_{CPMG})^{-1}$, where τ_{CPMG} is the 180° pulse spacing, and in (b,c) ν is given by $\nu_e = \omega_e/2\pi$. In both cases the effective field is defined by the time in which the magnetization is rotated through 360°. Simulations are based on Equations 1 and 7, respectively, assuming an equally populated two-state model with a chemical shift difference of 1 ppm at 60 MHz ^{15}N frequency. Simulations were carried out using Mathematica (Wolfram, 1991).

to remain effectively aligned with the spin-lock field. The lower limit to the rf power depends on the chemical shift differences in hertz, which are favorable for ^{15}N, thanks to its gyromagnetic ratio. An upper limit to the rf field is again given by the amount of power that can be transmitted to the probe and the sample. In practice experiments are performed in a working range of roughly $1000 \leq \nu_1 \leq 2500$ Hz (Banci et al., 1998). Since Equation 4 is obtained by a second order perturbation treatment, it applies only to cases for which $k_{ex} \gg \delta\omega$, i.e. fast exchange. Szyperski et al. (1993) have shown the application to the protein BPTI, and used variation of ω_1 in a ^{15}N $R_{1\rho}$ experiment to characterize a millisecond time scale event for Cys[38] and Arg[39]. Obviously, to investigate all the backbone ^{15}N nuclei in a protein having a typical chemical shift dispersion of about 2 kHz (not considering the side chain nitrogens of Arg, Lys and His), this method is impractical. Fortunately, the on-resonance condition is unneccesary and equally simple equations relate the observed relaxation rate in the presence of an rf field off-resonance to the parameters of the exchange process.

In the presence of a transverse spin-locking field, applied off-resonance by an amount $\Delta\omega = 2\pi\Delta\nu$, the spins will be quantized parallel to the effective field $\omega_e = 2\pi\nu_e = \sqrt{(\omega_1^2 + \Delta\omega^2)}$, which makes an angle $\theta = \tan^{-1}(\omega_1/\Delta\omega)$ with the laboratory frame z-axis. The relaxation rate along the effective field in the laboratory frame can be obtained *via* transformation to a doubly rotating frame and is given by Equation 12 of Jones (1966) for homonuclear spins, and by Equation 19 of Peng et al. (1991a) for heteronuclear spins. Using straightforward algebra it can be shown that their results reduce to:

$$R_{1\rho} = R_1 \cos^2\theta + R_2 \sin^2\theta \qquad (5)$$

under conditions $\omega_e \ll \omega_0 = \gamma B_0$ and $\omega_e\tau_c \ll 1$ for the interactions under consideration (Cornell and Pope, 1974). These requirements are met for dipolar and CSA interactions in proteins, where τ_c represents the internuclear reorientational correlation time, and

R_1 and R_2 correspond to the well-known expressions for the relaxation rates in the laboratory frame (see, for example, Abragam, 1961; Wagner, 1993). Since $\omega_e\tau_c \ll 1$ the values of R_1 and R_2 are themselves independent of the angle θ and are sufficient to describe the observed off-resonance relaxation rate.

In the case of exchange-mediated relaxation, where the condition $\omega_e\tau_{ex} \ll 1$ is violated, the density matrix approach of Jones (1966) may still be followed if $\delta\omega\tau_{ex} \ll 1$ (note that here τ_c is replaced by τ_{ex}, the exchange correlation time). This condition is identical to that used in the derivation of Equation 4 (Deverell et al., 1970). The resultant expression is again obtained via transformation to a doubly rotating frame (Davis et al., 1994; Desvaux et al., 1995), and $R_{2,ex}$ can be incorporated as an additional contribution to the transverse relaxation rate:

$$R_{1\rho} = R_1 \cos^2\theta + (R_2 + R_{2,ex}) \sin^2\theta \qquad (6)$$

with

$$R_{2,ex} = p_A p_B \delta\omega^2 \frac{k_{ex}}{k_{ex}^2 + \omega_e^2}, \qquad (7)$$

As can be seen from Equation 7, $R_{2,ex}$ bears an additional dependence on θ, through the strength of the effective field $\omega_e = \omega_1/\sin\theta$. Therefore, in the presence of chemical exchange, the exact value of $R_{1\rho}$ will also be determined by the parameters of the exchange process. The advantage of moving the rf field off-resonance is obvious when comparing Equations 4 and 7: with the same amount of rf power faster exchange processes can be studied. Although the effective field strength is, in principle, unlimited, exceedingly small values of τ_{ex} can, however, not be determined, due to the concomitant scaling of the exchange-mediated relaxation contribution by $\sin^2\theta$. In effect, as noted by Desvaux et al. (1995), for all values of ω_1 and τ_{ex} the relaxation contribution $R_{2,ex}\sin^2\theta$ is maximal for $\theta = \pi/2$. Consequently, by moving the rf field away from the resonances, values of k_{ex} can be obtained that are larger by roughly an order of magnitude than those obtainable by variation of the strength of the rf field alone (Cornell and Pope, 1974). In practice experiments were performed in a working range of $1800 \leq \nu_e \leq 9300$ Hz, using a constant level of the rf power at each offset. At these values of the effective field complications that arise because the resonance frequencies of the individual conformations differ are negligible.

The dependence of $R_{2,ex}$ on $\nu_e = \omega_e/2\pi$ and k_{ex} is illustrated in Figure 1. Panel b shows a contour plot of Equation 7 as a function of the effective field and exchange rate. The main characteristics are illustrated by horizontal and vertical cross sections depicted as dashed lines in panels c and d, respectively. The qualitative discussion for exchange-mediated relaxation in the presence of pulsed rf fields given above is equally appropriate here, and discussed in more detail in the next section. When the rf field is applied on-resonance, Equation 7 reduces to the familiar result obtained by Deverell et al. (1970), Equation 4, and in the limit that the rf field is removed one obtains the free-precession limit, Equation 3.

The combination of spin-echo and spin-lock measurements

As can be seen from Figure 1 the three-dimensional surfaces representing the chemical exchange contribution to the transverse relaxation in spin-echo and spin-locked measurements are strikingly similar. Of course, this result is not surprising as the effect of both methods is to reduce the fanning out of the magnetization vectors. The choice of the definition of ν_{CPMG} is obvious when considering that the spin-echo pulse train ultimately transforms into a spin-lock pulse in the limit of rapid pulsing.

In Figure 1c Equations 1 and 7 have been plotted as a function of the effective field for $k_{ex} = 10^4$ s^{-1}. Clearly, although the two methods share a high degree of similarity, experimental data can only be analyzed accurately by explicitly taking the forms of Equations 1 and 7 into account. The ranges of the experimental sampling provided by the spin-echo and spin-lock methods are illustrated. Although it is impossible or impractical to achieve extended sampling with either method, for reasons already mentioned, the complementarity of the sampling provided by the two methods is immediately obvious. Thus, a simultaneous way of analyzing CPMG and rotating frame relaxation rates allows for extensive sampling of the intermediate time scale motion.

Improved sampling can also be obtained by alternative hybrid methods, such as the combination of relaxation measurements in the presence of on-resonance and off-resonance rf fields (Banci et al., 1998). However, CPMG experiments seem to be better suited to measure relaxation in the presence of weak effective fields, for reasons mentioned above.

Alignment of the nuclear spin magnetization with the effective field in off-resonance rotating frame relaxation experiments

The demand to simultaneously determine ^{15}N off-resonance relaxation rates for all the nitrogen spins in a protein has led to the development of novel pulse sequences. The first to describe such an approach were Akke and Palmer (1996), who used a combination of high power rf pulses to transfer chemical shift offset evolution into the xz-plane. However, depending on the desired rotation angle and the offset frequencies of the spins, misalignment may occur, resulting in oscillations about the effective field and loss of magnetization. Therefore, adiabatic rotations were deemed more suitable. The use of trapezoidal amplitude modulation of the off-resonance rf field was exploited by Desvaux and co-workers (Zinn-Justin et al., 1997), who were able to achieve good alignment up to $\theta \approx 55°$. Larger rotations can, however, not be achieved by linear amplitude ramping alone, as the spin magnetization is not able to keep up with the rate of change of the effective field (a situation also referred to as 'violation of the adiabatic condition'). This problem can easily be overcome by simultaneous sweeping of the frequency of the rf field. We have recently shown (Mulder et al., 1998) that by a combination of hyperbolic tangent amplitude and tangent frequency modulation functions (Garwood and Ye, 1991) all spins can be properly aligned with the appropriate effective field, for all values of the angle θ.

Materials and methods

NMR spectroscopy

NMR experiments were performed on a Bruker AMX/2 600 spectrometer, operating at 600.14 MHz ^{1}H frequency. Spectra were acquired at 25 °C probe temperature on a 1.5 mM sample of uniformly ^{15}N labeled protein at pH 6.8 in 95/5 H_2O/D_2O v/v. The construct used was a C195A mutant of the RXR DBD, residues 130 to 209. The protein samples contained Cd rather than Zn, which, together with the cysteine substitution, drastically improved long term stability.

Relaxation measurements

Relaxation measurements were performed using adaptations of pulse sequences described by Dayie and Wagner (1994), including gradients for coherence selection in conjunction with sensitivity enhancement. Spectra were processed with NMRPipe (Delaglio et al., 1995) and analyzed using the in-house developed analysis tool REGINE (Kleywegt, 1991). Data sets were typically acquired as 128 × 512 complex points in the $t_1 \times t_2$ dimensions, with spectral widths of 2000 and 10000 Hz in F1 and F2, respectively. Lorentzian-to-Gaussian transformation and shifted, truncated sine-bell apodization (closely approximating Kaiser apodization functions) were employed in t_2 and t_1, respectively, prior to Fourier transformation. The resultant spectra, containing 512 × 2048 real points in the F1 × F2 dimensions, were of sufficient resolution to resolve all observable resonances. Peak intensities were represented by a summation over nine points to reduce the noise level. R_1, R_2 and $R_{1\rho}$ data points were fitted as a function of the length of the parametric relaxation delay to two-parameter decay curves of the form $I(t) = I_0 \exp(-Rt)$, using Levenberg–Marquardt minimization (Press et al., 1992). The error in the rate constant was assessed from 500 Monte Carlo simulations.

Heteronuclear ^{15}N{^{1}H} NOE were determined from the ratio of two experiments: (a) establishing nitrogen Zeeman polarization, and (b) creating nitrogen steady state magnetization under conditions of proton saturation. To avoid potential differential heating effects ^{1}H irradiation was performed in both experiments; (a) by off-resonant (100 kHz) continuous wave, or (b) by low power WALTZ-16 decoupling, positioning the carrier in the center of the amide proton region. The relaxation delay was 5 s in both cases, applying the proton rf pulses during the final 3 s. To compensate for possible long term spectrometer instabilities that may influence the experimental intensities the two experiments were recorded in triplicate, acquiring 16 scans per FID in each of the experiments. The total acquisition time was 36 h.

Spin-lattice relaxation times were determined from the time course of eight values of the parametric relaxation delay. In alternate measurements either $+N_z$ or $-N_z$ was created, and the resultant FIDs were subtracted to ensure exponential decay to zero intensity. Relaxation interference during the relaxation period was suppressed by ^{1}H spin saturation pulses (Boyd et al., 1990). Relaxation delays were 100 (2×), 200, 300, 400 (2×), 500, 600, 800 and 1000 ms. The total acquisition time for the entire series was 36 h, collecting 48 scans per FID.

CPMG spin-spin relaxation times were obtained employing six different spacings of the spin-echo pulse train and eight values of the parametric relax-

ation delay. ^{15}N spin-echo pulse spacings, τ_{CPMG}, were 400, 480, 640, 800, 960 and 1120 μs, corresponding to CPMG field strengths, ν_{CPMG}, of 1250, 1042, 781, 625, 521 and 446 Hz, respectively. At these values $\nu_{CPMG} \geq 5J$ to ensure that the decay is governed by the relaxation rate of the in-phase component. ^{15}N and ^{1}H 180° pulses were 62 μs and 20 μs, respectively. The use of short spin-echo pulses is desirable to minimize off-resonance effects (Ross et al., 1997). Relaxation delays varied from 10 to 120 ms, the exact values depending on τ_{CPMG}. DD/CSA relaxation interference during the relaxation period was suppressed by ^{1}H spin inversion at every even echo of the ^{15}N CPMG train (Kay et al., 1992; Palmer et al., 1992). At the lowest pulse repetition rate the ^{1}H 180° pulses were spaced by 4.48 ms, still sufficiently rapid to ensure a mono-exponential decay (Palmer et al., 1992). Duty cycle compensation was achieved by a very far off-resonant (100 kHz) CPMG block at the beginning of the pulse sequence to ensure the same amount of rf power dissipated into the sample for each relaxation delay. The total acquisition time for the entire series was 68 h, collecting 16 scans per FID and 96 complex points in F1.

Off-resonance rotating frame relaxation experiments were performed with simultaneous amplitude and frequency modulated adiabatic pulses as described previously (Mulder et al., 1998), using the pulse sequence as deposited with the BioMagResBank at the University of Wisconsin (URL: http://www.bmrb.wisc.edu). The rotating frame spin-lattice relaxation times were obtained employing eight different offsets of the off-resonance rf field and eight values of the parametric relaxation delay. The spin-lock field strength employed was 1800 ± 90 Hz and the off-resonance rf field was placed at 116.67, 111.74, 106.8, 100.23, 93.65, 83.79, 67.34, 50.90 and −14.87 ppm ($\Delta\omega_c/2\pi$ = 0, −300, −600, −1000, −1400, −2000, −3000, −4000 and −8000 Hz from the center of the nitrogen spectrum, respectively). These offsets correspond to nominal tilt angles $\Theta = \tan^{-1}(\omega_1/\Delta\omega_c)$ of 90.0, 80.5, 71.6, 61.0, 52.1, 42.0, 31.0, 24.2 and 12.7 degrees, and nominal effective field strengths $\Omega_e = \sqrt{(\omega_1^2 + \Delta\omega_c^2)}$ of 11.3, 11.5, 11.9, 12.9, 14.3, 16.9, 22.0, 27.6 and 51.5 krad/s, respectively. Adiabatic pulses were 4 ms, with a 25 kHz frequency sweep, using tanh/tan amplitude/frequency modulation functions. Relaxation delays were 10, 20, 30 (2×), 50, 70, 100 (2×), 150 and 200 ms. Relaxation interference during the relaxation period was suppressed by ^{1}H spin inversion every 5 ms (Kay et al., 1992; Palmer et al., 1992). The total acquisition time for the entire series was 68 h, collecting 8 scans per FID.

Fitting procedure

The experimentally obtained spin-echo and off-resonance relaxation rates were fit simultaneously by minimization of the χ^2 error function

$$\chi^2 = \sum_{i=1}^{n} \frac{(R_{2,i}^{exp} - R_{2,i}^{calc})^2}{\sigma_i^2} + \sum_{j=1}^{m} \frac{(R_{1\rho,j}^{exp} - R_{1\rho,j}^{calc})^2}{\sigma_j^2} \quad (8)$$

where n and m are the number of experimental R_2^{exp} and $R_{1\rho}^{exp}$ values, respectively, and σ are the uncertainties in the experimental values, obtained from Monte Carlo analyses. Values for R_2^{calc} were obtained using Equation 1 as model function, with the additon of the constant contribution to R_2 due to DD and CSA. Values for $R_{1\rho}^{calc}$ were obtained from Equation 6. In the absence of exchange, minimizing χ^2 required two parameters, R_1 and R_2. In the presence of exchange four parameters needed to be optimized: R_1, R_2, δω and k_{ex}. Since $p_A p_B \delta\omega^2$ cannot be delineated at a single value of the static field strength, it was assumed that $p_A = p_B = 0.5$. This yields a lower limit for δω in the case of unequal populations. To decrease the number of adjustable parameters to be included in the fitting, R_1 was fixed by the value obtained from the independent measurement. We noted, as others did (Akke and Palmer, 1996; Zinn-Justin et al., 1997; Akke et al., 1998), that, since the exchange-mediated relaxation contribution may be small, discriminating between models with and without exchange is delicate, and is greatly helped when the value of R_2 due to dipolar and CSA relaxation is obtained by alternative methods. Unfortunately, values of R_2 free of exchange contributions are difficult to obtain experimentally. Therefore, following the procedure suggested by Akke and Palmer (1996), R_2 was restrained during the minimization to a value calculated using the model-free formalism of Lipari and Szabo (1982), from experimental R_1 and heteronuclear NOE data. Since RXR is not spherical, local correlation times were obtained for each residue from a quadric analysis (vide infra). Consequently, the quality of the fit to the second model expresses whether the assumption of a single exchange event can be considered appropriate. With the possible exception of the three C-terminal residues, calculation

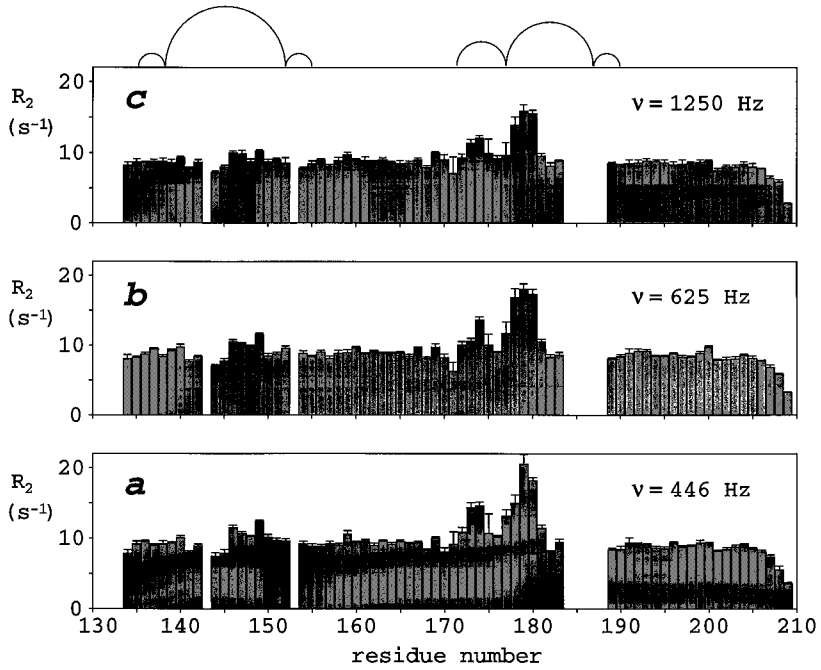

Figure 2. Bar graph of the experimental CPMG relaxation rates for RXR as a function of residue number. Panels a–c correspond to values of the CPMG field strength of 446, 625 and 1250 Hz, respectively. Artwork at the top of the figure indicates the positions of the loops and coordinating cysteine residues for both zinc finger domains.

of the transverse relaxation rates from the Lipari-Szabo analysis appeared to be a good approximation, as the values of R_1 and the heteronuclear NOE were very homogeneous over the sequence, so no large excursions of the backbone amides were expected. Thus, the number of adjustable parameters in the minimization of χ^2 was reduced to 1 (R_2) and 2 ($\delta\omega$ and k_{ex}) for models excluding and including chemical exchange, respectively. Error limits on the parameters were obtained from a Monte Carlo analysis of 200 synthetic data sets. Improvement of the fit by the more complicated model was obtained from the inspection of the reduced χ^2 values, χ^2_ν, and considered statistically significant if χ^2_ν (model 1) / χ^2_ν (model 2) > 1.7.

Results and discussion

To ensure the validity of our conclusions for the system under investigation, it was checked that Cd and Zn containing samples yielded essentially identical ^{15}N transverse relaxation rates, indicating that the same residues are involved in slow dynamics in both forms. Moreover, the Cd- and Zn-forms also exhibited enhanced ^{1}H transverse relaxation rates for the same residues. Residues Arg^{184}, Asn^{185}, Arg^{186}, Cys^{187} and Gln^{188} could not be observed in the ^{15}N-^{1}H correlation spectra. Measurements performed at 3 °C employing a water flip-back strategy to avoid saturation transfer from H_2O yielded only few additional cross peaks, belonging to arginine side chain N^ε-H^ε resonances. As arginine side chain protons are generally much more labile than backbone amide groups it was concluded that the missing resonances were broadened beyond detection by intermediate time scale dynamics, rather than saturated by exchange with the solvent.

^{15}N CPMG R_2 and off-resonance $R_{1\rho}$ relaxation data

The results of the CPMG R_2 measurement for several values of ν_{CPMG} are shown in Figure 2. In panel b the data obtained with a commonly used echo spacing of 800 μs is presented, and panels a and c present the data obtained with the minimal and maximal pulse repetition rate employed, respectively. The transverse relaxation rate is fairly homogeneous over the protein sequence, with the exception of a restricted number of sites. First, appreciable reduced values are found for the C-terminus (residues Glu^{207}-Arg^{209}), indicating the presence of fast (ps-ns) internal dynamics. Second, significantly enhanced transverse relaxation rates are observed for segments in the second zinc finger (residues Asp^{173}-Asn^{174} and Cys^{177}-Lys^{181}), indica-

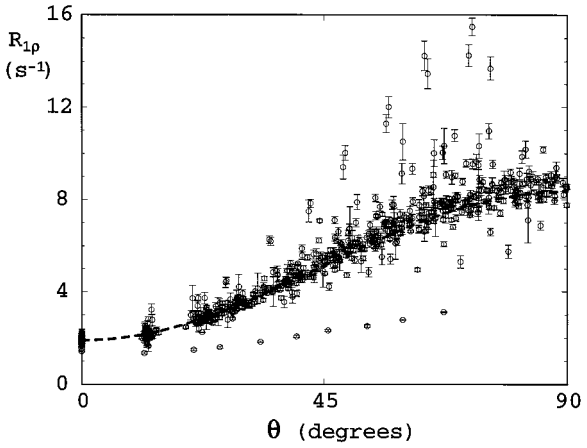

Figure 3. Plot of the experimental off-resonance rotating frame relaxation rates for RXR as a function of the angle θ with the laboratory frame z-axis. Data points are shown for each residue as a function of the tilt angle. Experimental R_1 data points are also shown ($\theta = 0$). The thick dashed curve was calculated from Equation 5 on the basis of the average experimental R_1 and R_2 values for the rigid body of the molecule.

tive of chemical exchange. When the data obtained for different values of the (CPMG)-field strength are compared (Figure 2a–c), it is obvious that, whereas the body of the molecule exhibits the same relaxation behavior over the entire regime of the pulse spacing, most of the elevated rates are decreased when the pulsing becomes more rapid. This is expected to occur when the pulse repetition rate becomes comparable in magnitude to the exchange rate (compare Figure 1). These data imply that the C-terminal residues exhibit structural disorder due to flexibility and that the second zinc finger exists as a number of interconverting species.

The results obtained in the off-resonance $R_{1\rho}$ experiment are shown in Figure 3. The data points represent the measured values of $R_{1\rho}$ for all residues, plotted as a function of the angle θ for each offset. The R_1 data have also been included in the plot, at $\theta = 0$. The black dashed line represents the theoretical curve according to Equation 5, using the average values of R_1 and R_2 for the non-mobile residues. Good agreement between the theoretical average curve and the experimental values is obtained for the majority of residues, reflecting the rigid part of the molecule. Two classes of residues deviate from this curve due to their dynamic nature: (i) residues exhibiting much lower relaxation rates over the entire range of the angle θ, corresponding to regions that are flexible on the ps-ns time scale, and (ii) residues showing increased relaxation rates, indicating the presence of μs-ms dynamics. Not surprisingly, the deviant residues are identical to those already identified from the CPMG data.

To check the consistency of CPMG and off-resonance relaxation data, the average values of $R_{1\rho}$ and R_2 were compared. To obtain the 'true' on-resonance transverse relaxation rates from the $R_{1\rho}$ data, values obtained at a nominal offset of 0 Hz were corrected for the resonance offset of the individual spins on the basis of Equation 5, using the experimentally determined R_1 data. For a representative CPMG R_2 data set the values obtained with 800 μs echo spacing were used. Excluding the termini and the zinc finger regions, the average CPMG R_2 and on-resonance $R_{1\rho}$ values were 8.63 ± 0.46 s^{-1} and 8.66 ± 0.38 s^{-1}, respectively. It was concluded that the measurements were indeed indistinguishable and could be used as complementary data.

Analysis of chemical exchange

Simultaneous fitting of the ^{15}N CPMG R_2 and off-resonance $R_{1\rho}$ relaxation data, with R_2 as the sole adjustable parameter, resulted in a low average reduced χ^2, indicating that many residues could be fitted satisfactorily to a model without exchange. However, several residues had strongly elevated values of χ^2, indicating that data and model were not in agreement. Subsequently, the data for all residues were fitted with k_{ex} and δω as adjustable parameters. For 14 residues the reliability of the model improved considerably by the inclusion of exchange, as judged from the reduced χ^2 ratio. The values of τ_{ex} and δω obtained are presented in Table 1. Microsecond time scale dynamics were almost exclusively observed for loop regions, with the exception of a few isolated cases. Specifically, flexibility is observed for three contiguous segments, comprising residues His^{146} to Val^{149} of the first zinc finger region, Lys^{165} to Leu^{167} of the extended region following the second helix, and Cys^{177} to Asp^{180} of the second zinc finger domain. A comparison of the raw and analyzed data immediately makes clear the need to rely on both spin-echo and spin-lock measurements for the identification of slow motions: whereas several exchanging residues were readily identified from the anomalous increase in R_2, a large number was not. There may be two reasons for this: (i) the chemical shift difference in such cases is relatively small (< 1 ppm) and, in combination with rate constants that greatly exceed the shift difference, the exchange-mediated relaxation contribution will be

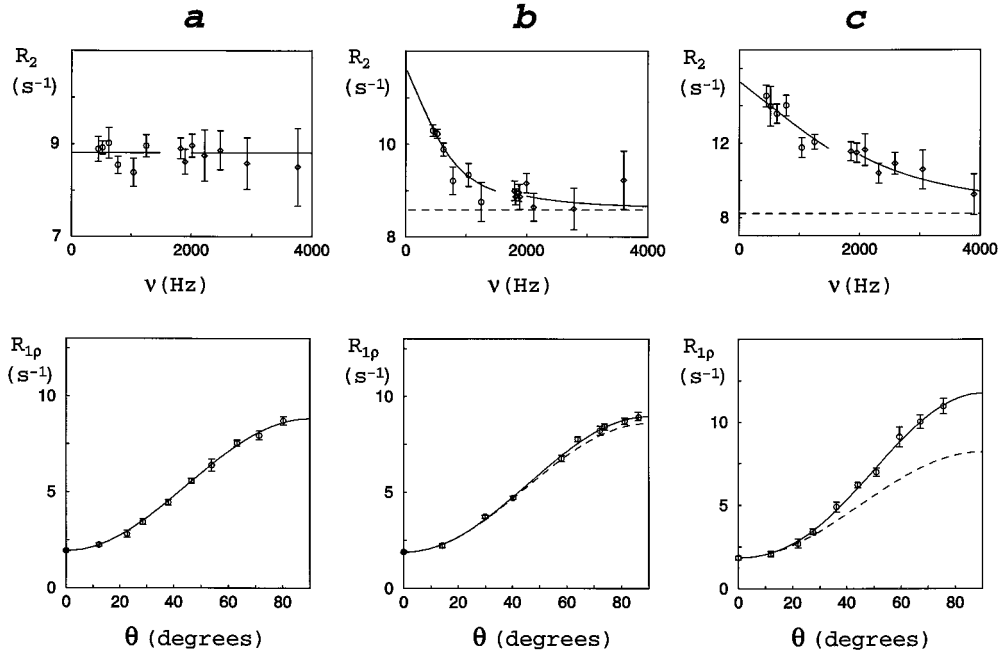

Figure 4. Plots of experimental and fitted CPMG R_2 and off-resonance $R_{1\rho}$ data for residues Lys^{156} (a), Gly^{148} (b) and Asn^{174} (c). Bottom panels represent spin-lock relaxation data as a function of the tilt angle. Top panels give the values of R_2 from the CPMG experiment and those calculated from the $R_{1\rho}$ data. Full curves represent the best fits to the data. Dashed curves indicate the exchange-free R_2 value, calculated from R_1 and the heteronuclear NOE. The results for Lys^{156} (helix I) are representative for residues in the core of the protein, which did not require an exchange contribution. The results for residues Gly^{148} (first zinc finger domain) and Asn^{174} (D-box of the second zinc finger domain) illustrate how the model including microsecond time scale dynamics better describes the experimental data for these residues. Values of the reduced χ^2 were 0.57, 0.99 and 0.72, respectively.

small, or (ii) the identification of intermediate time scale motions may be precluded by the simultaneous presence of fast dynamics, which has an opposing effect on the relaxation rate. Although small, the relaxation dispersion can obviously still be measured with the experiments presented and a picture of the intrinsic dynamics is obtained. Conversely, several residues having values of R_2 that are more than 1 s^{-1} higher than that calculated from R_1 and the heteronuclear NOE, such as Tyr^{150}, Arg^{172}-Asp^{173}, Lys^{181} and Arg^{191}, had average values of χ^2 and did not improve significantly with the second model. This implies that the transverse relaxation rate showed little dispersion for the currently sampled values of the effective field strength. Such a case can be explained by exchange rates that considerably exceed both the chemical shift difference and the effective field strength, indicating the presence of dynamic processes with rate constants as large as 10^5 s^{-1}. Alternatively, residues Ala^{136}, Ser^{142}, Lys^{201} and Arg^{209} failed to comply with either model (lowest $\chi^2_\nu \approx 6$). This may be due to exchange on multiple time scales, or, alternatively, the explanation could lie with the use of restrained values of R_2 from a model-free analysis. Indeed, the model invoked by the model-free formalism may not be adequate, and such a failing would primarily manifest itself for flexible residues. This shortcoming calls for obtaining exchange-free values of R_2 by alternative methods, for example from the analysis of cross-correlated relaxation rates (Kroenke et al., 1998). Nonetheless, in the present case the residues requiring an exchange contribution were not very flexible as judged from the R_1 and heteronuclear NOE data, and it is believed that the exchange parameters reported accurately describe the intermediate time scale dynamics for RXR.

Representative experimental data and fitted curves are shown for three residues in Figure 4. For each residue the off-resonance $R_{1\rho}$ data points are shown in the bottom panel, and the R_2 values from the CPMG experiment and those calculated from the $R_{1\rho}$ data are shown in the top panels. Full and dashed curves correspond to models including and excluding exchange contributions, respectively. Curves through the CPMG and off-resonance data are shown separately, and were

Table 1. Exchange time constants and chemical shift differences for intermediate time scale dynamics in RXR obtained from ^{15}N CPMG R_2 and off-resonance $R_{1\rho}$ relaxation

Residue	τ_{ex} (μs)[a]	$\delta\nu$ (ppm)[a]	R_{ex} (s^{-1})[b]
His^{146}	58 ± 11	1.25 ± 0.08	2.54
Tyr^{147}	51 ± 13	1.06 ± 0.10	1.48
Gly^{148}	220 ± 40	0.60 ± 0.02	–
Val^{149}	83 ± 7	1.23 ± 0.03	2.30
Tyr^{150}	–	–	1.46
Lys^{165}	416 ± 209	0.49 ± 0.34	–
Asp^{166}	193 ± 49	0.41 ± 0.02	–
Leu^{167}	131 ± 21	0.60 ± 0.03	–
Arg^{172}	–	–	1.15
Asp^{173}	–	–	4.36
Asn^{174}	87 ± 9	1.51 ± 0.04	3.44
Cys^{177}	142 ± 57	0.98 ± 0.22	2.20
Leu^{178}	53 ± 6	2.26 ± 0.06	7.40
Ile^{179}	37 ± 7	2.90 ± 0.21	8.17
Asp^{180}	38 ± 5	2.69 ± 0.15	8.38
Lys^{181}	–	–	2.21
Arg^{191}	–	–	1.05
Leu^{196}	248 ± 67	0.43 ± 0.10	–
Met^{198}	134 ± 28	0.48 ± 0.02	–

[a]Residues have been tabulated for which χ^2_ν (model 1) / χ^2_ν (model 2) > 1.7.
[b]R_{ex} obtained from Lipari-Szabo analysis. All residues with $R_{ex} > 1.0\ s^{-1}$ are tabulated.

calculated from the optimized parameters, using Equations 1 and 7, respectively. Panels a illustrate the results obtained for Lys^{156}, a representative residue for the core of the protein. As expected, the R_2 data fall onto a horizontal line and the off-resonance $R_{1\rho}$ data obey the simple relationship of Equation 5. Panels b represent the data for residue Gly^{148} of the first zinc finger domain. Owing to its relatively large value of τ_{ex} (220 μs), a typical concave R_2 decay is observed, whereas the off-resonance relaxation rates – described by Equation 6 – are barely affected. In panels c the results are shown for residue Asn^{174} in the D-box of the second zinc finger domain. For this residue τ_{ex} is relatively small (87 μs) and, consequently, its R_2 relaxation curve shows an almost linear dependence on ν for the CPMG data. In this case large additional contributions to the rotating frame relaxation rates are observed, with significant dispersion as a function of the effective field.

Comparison with model-free parameters

The analysis of ^{15}N heteronuclear relaxation data in terms of the well-known model-free formalism (Lipari and Szabo, 1982) was carried out following the procedure described by Li and Montelione (1995), using the offset-corrected values of the $R_{1\rho}$ experiment at 0 Hz offset as transverse relaxation data set. However, since RXR is subject to anisotropic rotational diffusion, local correlation times were used for each residue, obtained from a quadric analysis (Brüshweiler et al., 1995) of the experimentally obtained R_1 and R_2 data, following the procedures described by Lee et al. (1997). The analysis was based on data for 54 residues, excluding those that are part of the zinc finger subdomains and the C-terminus. Calculations were done using a representative member of the ensemble of NMR solution structures (structure 20 of PDB entry 1rxr.pdb). The diffusion tensor is axially symmetric, with $D_{iso} = 2.78 \times 10^7\ s^{-1}$, and $D_{par}/D_{per} = 0.84$. The improvement in the fit for an axially symmetric model compared with an isotropic model is given by $F = 11.1$; $p = 1.0 \times 10^{-3}$. A slight further improvement in the fit when including totally anisotropic diffusion ($F = 2.16$; $p = 0.12$) was not considered significant. The resultant values of the exchange contribution are given in Table 1. Treating values of $R_{2,ex}$ larger than $1.0\ s^{-1}$ as significant for the presence of exchange, the resultant data fall into three categories: (i) residues having large exchange contributions, which were also identified from the relaxation dispersion, such as His^{146}, Tyr^{147}, Val^{149}, Asn^{174} and the segment Cys^{177}-Asp^{180}, having rate constants on the order of $10^4\ s^{-1}$ and standing out for chemical shift differences larger than 1 ppm; (ii) residues with large exchange contributions, which did not show significant dispersion in the relaxation rate, comprising Tyr^{150}, Arg^{172}-Asp^{173}, Lys^{181} and Arg^{191}. These residues likely exhibit rate constants on the order of $10^5\ s^{-1}$ and chemical shift perturbations that exceed 1 ppm (compare Equation 3); and (iii) residues for which no intermediate time scale motions were inferred on the basis of $R_{2,ex}$, but which show transverse relaxation rates that are dependent on the effective field strength. These residues were overlooked due to the small chemical shift differences (≈ 0.5 ppm). The present experiments and data analysis are, however, capable of providing conclusive evidence for the presence of dynamics in such cases (compare Table 1).

Structural fluctuation and function of RXR DBD

Nuclear receptors interact with their cognate hormone response elements (HREs) through highly conserved DNA-binding domains. Members of the TR receptor subfamily, such as VDR, TR and RAR, form heterodimers with RXR, which acts as a common factor for high affinity binding. The receptor specificity is largely determined by the HREs, made up of direct repeats (DRXs) of AGGTCA, with a varying number (X) of bases in the spacer between the hexanucleotides (see, for example, Mangelsdorf and Evans, 1995). The DBDs of the nuclear receptor proteins bind to the DNA in a head-to-tail arrangement, with RXR occupying the 5′ (downstream) position, bringing distinct regions of each DBD to their dimerization interface. Due to the variation in spacer length RXR cannot interact with a common interface in each of its partners. Rather, it must possess a series of nested surfaces that correspond to the rotational and distance changes of its partners. It was suggested that the RXR DBD acts as a type of gear allowing sprockets (amino acids) from the downstream subunit to be engaged only in the appropriate alignment (Mangelsdorf and Evans, 1995). The dimerization interfaces of RXR with VDR, TR and RAR on DR3, DR4 and DR5, respectively, exclusively involve the second finger region of RXR, including the D-box (Zechel et al., 1994b; Rastinejad et al., 1995). In addition, RXR can also homodimerize on DR1 and heterodimerize with RAR on DR2 response elements, allowing yet other portions of the second zinc finger domain and also the C-terminal T-box to engage in the dimer interface (Zechel et al., 1994a). If RXR were a rigid protein, all its complementary dimerization surfaces should simultaneously be present in a single structure. NMR structural studies of RXR free in solution (Lee et al., 1993; Holmbeck et al., 1998) indicated that, whereas the helices form a well-defined protein scaffold, the zinc-binding domains exhibit considerable disorder. The crystal structure of RXR, complexed with TR on a DR4 response element, revealed that in nuclear receptor assembly the second finger is no longer dynamic but forms a distorted helix, allowing the interacting residues to become correctly positioned in the interface (Rastinejad et al., 1995). Our relaxation data confirm that RXR consists of a rigid core, with major structural fluctuations occurring in the second zinc finger. The presence of a dynamic dimerization domain alleviates the requirement of a prefabricated structural array, and, rather, suggests a more flexible picture of nuclear receptor assembly on DNA direct repeats. This result may be used to explain how RXR, through the ability to adaptively interact with a wide variety of highly homologous partner molecules, demonstrates such a versatile DNA-binding repertoire.

The presence of disorder in the dimerization domain is reminiscent of the situation found for the steroid hormone receptors GR and ER, which bind as homodimers to DNA inverted repeats. The dimerization domain (D-box) of the proteins free in solution is ill-defined, and becomes structured in the ternary complexes (Luisi et al., 1991; Schwabe et al., 1993; Tilborg et al., 1995). Flexibility obviously provides the protein modules with the ability to induce the correct fold for the dimer interface, facilitating the cooperative interaction between monomers on binding to DNA.

Conclusions

It was demonstrated that, from an account of the theory of chemical exchange in the presence of spin-echo or spin-lock rf pulses, CPMG R_2 and off-resonance $R_{1\rho}$ experiments are excellent complements to achieve an extended sampling of microsecond time scale dynamics. Whereas the equations, relating the observed relaxation rate to the parameters of the exchange process, are very distinct for the two cases, their appearance is strikingly similar when represented as a function of the effective field strength, ν_{CPMG} or ν_e, defined by the rate of rotation of the nuclear spin magnetization. Application of ^{15}N CPMG R_2 and off-resonance $R_{1\rho}$ relaxation experiments to RXR DBD allowed the identification of 14 residues exhibiting intermediate time scale dynamics, and the values of the exchange parameters, k_{ex} and $\delta\omega$, have been determined for each individual residue.

The present data report microsecond time scale dynamics occuring in the zinc-finger domains of RXR. Major disturbances of tertiary structure are inferred for residues Leu^{178}, Ile^{179} and Asp^{180} of the second zinc-coordinating domain. Structural fluctuations in this region agree with disorder in previously reported NMR solution structures (Lee et al., 1993; Holmbeck et al., 1998). Since the second zinc-finger domain comprises the principal dimerization interface in a wide repertoire of complexes with different hormone receptors to their cognate response elements, our results may be used to explain the promiscuity observed for RXR. A picture emerges of a flexible zinc-containing domain that has been engineered to establish a highly adaptable binding surface for a wide variety of cooperative

interactions between nuclear receptor monomers on DNA assembly.

Acknowledgements

We thank Maaike de Backer and Dr. Margie Nair for carrying out initial relaxation studies on RXR. We are indebted to Erika van Heerde, Drs. Paul van der Saag and Yasmin Karimi-Nejad for the ^{15}N enriched sample. Drs. Alexandre Bonvin and Hans Vis are acknowledged for contributions to the relaxation analysis software. We thank Alison Meekhof and Dr. Stefan Freund for stimulating discussions and a copy of their manuscript prior to publication. We also thank Dr. Peter Wright for sharing unpublished results. Dr. Gert Folkers is acknowledged for helpful comments. This work was supported by the Netherlands Foundation for Chemical Research (SON) with financial assistance from the Netherlands Organization for Scientific Research (NWO).

References

Abragam, A. (1961) *The Principles of Nuclear Magnetism*, Clarendon Press, Oxford.

Akke, M. and Palmer III, A.G. (1996) *J. Am. Chem. Soc.*, **118**, 911–912.

Akke, M., Liu, J., Cavanagh, J., Erickson, H.P. and Palmer III, A.G. (1998) *Nat. Struct. Biol.*, **5**, 55–59.

Allerhand, A. (1966) *J. Chem. Phys.*, **44**, 1–9.

Banci, L., Felli, I.C. and Koulougliotis, D. (1998) *J. Biomol. NMR*, **12**, 307–318.

Bloom, M., Reeves, L.W. and Wells, E.J. (1965) *J. Chem. Phys.*, **42**, 1615–1624.

Brüshweiler, R., Liao, X. and Wright, P.E. (1995) *Science*, **268**, 886–889.

Cornell, B.A. and Pope, J.M. (1974) *J. Magn. Reson.*, **16**, 172–181.

Davis, D.G., Perlman, M.E. and London, R.E. (1994) *J. Magn. Reson.*, **B104**, 266–275.

Dayie, K.T. and Wagner, G. (1994) *J. Magn. Reson.*, **A111**, 121–126.

Delaglio, F., Grzesiek, S., Vuister, G.W., Zhu, G., Pfeifer, J. and Bax, A. (1995) *J. Biomol. NMR*, **6**, 277–293.

Desvaux, H., Birlirakis, N., Wary, C. and Berthault, P. (1995) *Mol. Phys.*, **86**, 1059–1073.

Deverell, C., Morgan, R.E. and Strange, J.H. (1970) *Mol. Phys.*, **18**, 553–559.

Garwood, M. and Ke, Y. (1991) *J. Magn. Reson.*, **94**, 511–525.

Hirs, C.H.W. and Timosheff, S.N. (1986) *Methods Enzymol.*, **131**, 283–607.

Holmbeck, S.M.A., Foster, M.P., Casimiro, D.R., Sem, D.S., Dyson, H.J. and Wright, P.E. (1998) *J. Mol. Biol.*, **281**, 271–284.

Jacquinot, J.F. and Goldman, M. (1973) *Phys. Rev.*, **B8**, 1944–1957.

Jones, G.P. (1966) *Phys. Rev.*, **148**, 332–335.

Karplus, M. and McCammon, J.A. (1986) *Sci. Am.*, **254**, April, 42–51.

Kay, L.E., Nicholson, L.K., Delaglio, F., Bax, A. and Torchia, D.A. (1992) *J. Magn. Reson.*, **97**, 359–375.

Kleywegt, G.J. (1991) *Computer assisted Assignment of 2D and 3D NMR Spectra of Proteins*, Ph.D. Thesis, Utrecht University.

Kroenke, C.D., Loria, J.P., Lee, L.K., Rance, M. and Palmer III, A.G. (1998) *J. Am. Chem. Soc.*, **120**, 7905–7915.

Lee, M.S., Kliewer, S.A., Provencal, J., Wright, P.E. and Evans, R.M. (1993) *Science*, **260**, 1117–1121.

Lee, L.K., Rance, M., Chazin, W.J. and Palmer III, A.G. (1997) *J. Biomol. NMR*, **9**, 287–298.

Li, Y.-C. and Montelione, G.T. (1995) *Biochemistry*, **34**, 2408–2423.

Lipari, G. and Szabo, A. (1982) *J. Am. Chem. Soc.*, **104**, 4546–4559.

Luisi, B.F., Xu, W.X., Otwinowski, Z., Freedman, L.P., Yamamoto, K.R. and Sigler, P.B. (1991) *Nature*, **352**, 497–505.

Luz, Z. and Meiboom, S. (1963) *J. Chem. Phys.*, **39**, 366–370.

Mandel, A.M., Akke, M. and Palmer III, A.G. (1996) *Biochemistry*, **35**, 16009–16023.

Mangelsdorf, D.J. and Evans, R.M. (1995) *Cell*, **83**, 841–850.

Meekhof, A.E., Hamill, S.J., Arcus, V.L., Clarke, C. and Freund, S.M.V. (1998) *J. Mol. Biol.*, **282**, 181–194.

Meiboom, S. (1961) *J. Chem. Phys.*, **34**, 375–388.

Mueller, L., Legault, P. and Pardi, A. (1995) *J. Am. Chem. Soc.*, **117**, 11043–11048.

Mulder, F.A.A., Spronk, C.A.E.M., Slijper, M., Kaptein, R. and Boelens, R. (1996) *J. Biomol. NMR*, **8**, 223–228.

Mulder, F.A.A., de Graaf, R., Kaptein, R. and Boelens, R. (1998) *J. Magn. Reson.*, **131**, 351–357.

Orekhov, V.Y., Pervushin, K.V. and Arseniev, A.S. (1994) *Eur. J. Biochem.*, **219**, 887–896.

Palmer III, A.G., Rance, M. and Wright, P.E. (1991) *J. Am. Chem. Soc.*, **113**, 4371–4380.

Palmer III, A.G., Skelton, N.J., Chazin, W.J., Wright, P.E. and Rance, M. (1992) *Mol. Phys.*, **75**, 699–711.

Palmer III, A.G., Williams, J. and McDermott, A. (1996) *J. Phys. Chem.*, **100**, 13293–13310.

Peng, J.W. and Wagner, G. (1994a) In *Nuclear Magnetic Resonance Probes of Molecular Dynamics* (Tycko, R., Ed.), Kluwer Academic Publishers, Dordrecht, pp. 373–454.

Peng, J.W. and Wagner, G. (1994b) *Methods Enzymol.*, **239**, 563–596.

Peng, J.W., Thanabal, V. and Wagner, G. (1991a) *J. Magn. Reson.*, **94**, 82–100.

Peng, J.W., Thanabal, V. and Wagner, G. (1991b) *J. Magn. Reson.*, **95**, 421–427.

Phan, I.Q.H., Boyd, J. and Campbell, I.D. (1996) *J. Biomol. NMR*, **8**, 369–378.

Press, W.H., Flannery, B.P., Teukolsky, S.A. and Vetterling, W.T. (1992) *Numerical Recipes in C*, 2nd ed., Cambridge University Press, Cambridge, U.K.

Rastinejad, F., Perlman, T., Evans, R.M. and Sigler, P.B. (1995) *Nature*, **375**, 203–211.

Ross, A., Czisch, M. and King, G.C. (1997) *J. Magn. Reson.*, **124**, 355–365.

Schwabe, J.W.R., Chapman, L., Finch, J.T., Rhodes, D. and Neuhaus, D. (1993) *Structure*, **1**, 187–204.

Strange, J.H. and Morgan, R.E. (1970) *J. Phys. C: Solid St. Phys.*, **3**, 1999–2011.

Szyperski, T., Luginbühl, P., Otting, G., Güntert, P. and Wüthrich, K. (1993) *J. Biomol. NMR*, **3**, 151–164.

Torchia, D.A., Nicholson, L.K., Cole, H.B.R. and Kay, L.E. (1993) In *NMR of Proteins* (Clore, G.M. and Gronenborn, A.M., Eds.), Macmillan Press Ltd, London, pp. 190–219.

van Tilborg, M.A.A., Bonvin, A.M.J.J., Hård, K., Davis, A.L., Maler, B., Boelens, R., Yamamoto, K.R. and Kaptein, R. (1995) *J. Mol. Biol.*, **247**, 689–700.

van Tilborg, P.J.A., Mulder, F.A.A., de Backer, M.M.E., Nair, M., van Heerde, E., Folkers, G., van der Saag, P., Karimi-Nejad, Y., Boelens, R. and Kaptein, R. (1999) *Biochemistry*, in press.

Vis, H., Vorgias, C.E., Wilson, K.S., Kaptein, R. and Boelens, R. (1998) *J. Biomol. NMR*, **11**, 265–277.

Wagner, G. (1993) *Curr. Opin. Struct. Biol.*, **3**, 748–754.

Wagner, G., Hyberts, S. and Peng, J.W. (1993) In *NMR of Proteins* (Clore, G.M. and Gronenborn, A.M., Eds.), Macmillan Press Ltd, London, pp. 220–257.

Wishart, D.S., Sykes, B.D. and Richards, F.M. (1991) *J. Mol. Biol.*, **222**, 311–333.

Wolfram, S. (1991) *The Mathematica Book*, 3rd ed., Cambridge University Press, Cambridge, U.K.

Zechel, C., Shen, X.-Q., Chambon, P. and Gronemeyer, H. (1994a) *EMBO J.*, **13**, 1414–1424.

Zechel, C., Shen, X.-Q., Chen, J.-Y., Chen, Z.-P., Chambon, P. and Gronemeyer, H. (1994b) *EMBO J.*, **13**, 1425–1433.

Zinn-Justin, S., Berthault, P., Guenneugues, M. and Desvaux, H. (1997) *J. Biomol. NMR*, **10**, 363–372.